Cancer Research

Dynamic Mathematical Modeling of IL13-Induced Signaling in Hodgkin and Primary Mediastinal B-Cell Lymphoma Allows Prediction of Therapeutic Targets

Valentina Raia, Marcel Schilling, Martin Böhm, et al.

Updated Version	Access the most recent version of this article at: doi:10.1158/0008-5472.CAN-10-2987
Supplementary Material	Access the most recent supplemental material at: http://cancerres.aacrjournals.org/content/suppl/2010/12/02/0008-5472.CAN-10-2987.DC1.html

Cited Articles	This article cites 42 articles, 16 of which you can access for free at: http://cancerres.aacrjournals.org/content/71/3/693.full.html#ref-list-1

E-mail alerts	Sign up to receive free email-alerts related to this article or journal.
Reprints and Subscriptions	To order reprints of this article or to subscribe to the journal, contact the AACR Publications Department at pubs@aacr.org.
Permissions	To request permission to re-use all or part of this article, contact the AACR Publications Department at permissions@aacr.org.

Dynamic Mathematical Modeling of IL13-Induced Signaling in Hodgkin and Primary Mediastinal B-Cell Lymphoma Allows Prediction of Therapeutic Targets

Valentina Raia[1], Marcel Schilling[1], Martin Böhm[2], Bettina Hahn[2], Andreas Kowarsch[3], Andreas Raue[4], Carsten Sticht[5], Sebastian Bohl[1], Maria Saile[5], Peter Möller[6], Norbert Gretz[5], Jens Timmer[4,7,8], Fabian Theis[3], Wolf-Dieter Lehmann[2], Peter Lichter[9], and Ursula Klingmüller[1]

Abstract

Primary mediastinal B-cell lymphoma (PMBL) and classical Hodgkin lymphoma (cHL) share a frequent constitutive activation of JAK (Janus kinase)/STAT signaling pathway. Because of complex, nonlinear relations within the pathway, key dynamic properties remained to be identified to predict possible strategies for intervention. We report the development of dynamic pathway models based on quantitative data collected on signaling components of JAK/STAT pathway in two lymphoma-derived cell lines, MedB-1 and L1236, representative of PMBL and cHL, respectively. We show that the amounts of STAT5 and STAT6 are higher whereas those of SHP1 are lower in the two lymphoma cell lines than in normal B cells. Distinctively, L1236 cells harbor more JAK2 and less SHP1 molecules per cell than MedB-1 or control cells. In both lymphoma cell lines, we observe interleukin-13 (IL13)-induced activation of IL4 receptor α, JAK2, and STAT5, but not of STAT6. Genome-wide, 11 early and 16 sustained genes are upregulated by IL13 in both lymphoma cell lines. Specifically, the known STAT-inducible negative regulators *CISH* and *SOCS3* are upregulated within 2 hours in MedB-1 but not in L1236 cells. On the basis of this detailed quantitative information, we established two mathematical models, MedB-1 and L1236 model, able to describe the respective experimental data. Most of the model parameters are identifiable and therefore the models are predictive. Sensitivity analysis of the model identifies six possible therapeutic targets able to reduce gene expression levels in L1236 cells and three in MedB-1. We experimentally confirm reduction in target gene expression in response to inhibition of STAT5 phosphorylation, thereby validating one of the predicted targets. *Cancer Res; 71(3); 693–704. ©2010 AACR.*

Major Findings

We uncover major differential aberrations in the stoichiometry of JAK/STAT pathway components in the lymphoma-derived cell lines MedB-1 and L1236 compared with normal B cells. Furthermore, we identify that the IL13 decoy receptor and the induction of negative feedback regulators significantly contribute to IL13 signaling in MedB-1 cells but not in L1236. Finally, we show that our data-based mathematical models of the JAK/STAT pathway in lymphoma cells facilitate the quantitative prediction of perturbations, opening the possibility to guide the identification of therapeutic targets.

Introduction

A deregulated activation of JAK (Janus kinase)/STAT pathway is frequently observed in 2 clinically different hematologic malignancies: primary mediastinal B-cell lymphoma (PMBL) and classical Hodgkin lymphoma (cHL). The STAT family member STAT6 is hyperphosphorylated in about 80% of PMBL (1) and cHL (2) patients, mutations of the negative regulator *SOCS1* are common (3, 4) and chromosomal aberrations including gains of the *JAK2* gene were observed in 35% of PMBLs and in 33% of Hodgkin lymphomas (5). STAT5, another STAT family member, is phosphorylated in approximately 30% of cHL patients (6). In normal B cells, interleukin (IL)-13 and IL4 are the ligands inducing the activation of the pathway

Authors' Affiliations: [1]Divisions of Systems Biology of Signal Transduction, DKFZ-ZMBH Alliance and [9]Molecular Genetics, and [2]Molecular Structural Analysis, German Cancer Research Center (DKFZ), Heidelberg; [3]Computational Modeling in Biology, Institute for Bioinformatics and Systems Biology, Helmholtz Zentrum München; [4]Physics Institute, University of Freiburg; [5]Medical Research Center, Medical Faculty Mannheim, University of Heidelberg, Mannheim; [6]Institute of Pathology, Ulm University Clinic, Ulm; [7]Freiburg Institute for Advanced Studies; and [8]Centre for Biological Signalling Studies (BIOSS), University of Freiburg, Freiburg, Germany

American Association for *Cancer Research*

Quick Guide to Main Model Equations

Here we describe 2 key reactions of the MedB-1 model. A model description is in Supplementary Text S7. Details of MedB-1 and L1236 models are in Supplementary Text S8.

$$\text{pJAK2}: d(\text{pJAK2})/dt = \text{JAK2\_phosphorylation} \times \text{IL13\_Rec} \times \text{JAK2}/(1 + \text{JAK2\_p\_inhibition} \times \text{SOCS3})$$
$$+ \text{JAK2\_phosphorylation} \times \text{p\_IL13\_Rec} \times \text{JAK2}/(1 + \text{JAK2\_p\_inhibition} \times \text{SOCS3})$$
$$- \text{pJAK2\_dephosphorylation} \times \text{pJAK2} \times \text{SHP1}$$

The amount of pJAK2 over time is dependent on several factors because its production is triggered by either IL13_Rec or p_IL13_Rec and is inhibited by SOCS3 and SHP1. The equation describing pJAK2 behavior over time in our model is thus composed by the sum of 2 inducing reactions minus the SHP1-triggered reverse reaction pJAK2 → JAK2. SOCS3 contribution was introduced as a denominator to each of the 2 inducing reactions. The difference between SOCS3 and SHP1 lies in the fact that SOCS3 inhibits the phosphorylation of JAK2 whereas SHP1 induces the dephosphorylation of pJAK2.

$$\text{SOCS3}: d(\text{SOCS3})/dt = \text{SOCS3mRNA} \times \text{SOCS3\_translation}/(\text{SOCS3\_accumulation} + \text{SOCS3mRNA})$$
$$- \text{SOCS3\_degradation} \times \text{SOCS3}$$

The equation describing SOCS3 behavior over time is composed of 3 parts: (i) SOCS3mRNA-dependent SOCS3_production divided by (ii) SOCS3_accumulation summed to SOCS3mRNA minus (iii) SOCS3_degradation.

Major Assumptions of the Model

1) We assume that the initial value of all phosphorylated species in the model is 0, i.e., we assume that the starvation is 100% efficient. This assumption is supported by immunoblotting and MS evidence.
2) We assume that the initial value of *SOCS3* and *CD274* mRNA is zero.
3) We consider the cell as one compartment and we assume free spatial availability of all molecules to others.
4) We assume that the number of SHP1 molecules per cell is constant over time. This assumption is supported by IB evidence (Supplementary Fig. S9).
5) On the basis of previous works (30, 31), and because we could coimmunoprecipitate SHP1 with STAT5 and detect it by immunoblotting and MS analysis (Supplementary Fig. S10), we assume that SHP1 is responsible for the dephosphorylation of pSTAT5.
6) The species named "Rec" in the model is a heterodimer composed of IL4Ra and IL13Ra1. We assume that upon binding of IL13, the receptor complex can phosphorylate JAK2, because of its association with the kinase TYK2 (also included in "Rec").

mediated by the IL4 receptor α (IL4Ra), IL13 receptor α 1 (IL13Ra1), the associated kinases JAK2 and TYK2, and the transcription factors STAT5 and STAT6 (7, 8). In the tumor cells of cHL (Hodgkin and Reed-Sternberg cells), it has been shown that IL13 is secreted and stimulates the tumor cells in an autocrine manner (9).

Despite the extensive knowledge of alterations in the JAK/STAT pathway, several issues concerning its aberrant activation in lymphomas remained unresolved, including the role of nonmutated negative regulators, such as the inducible SOCS3 and the constitutively expressed SHP1. Furthermore, the differential role of STAT5 and STAT6 is still controversially discussed (1, 2, 4, 7, 10). Dealing with such complex, nonlinear systems, traditional qualitative or semiquantitative studies are not sufficient to understand dynamic properties and to quantitatively predict suitable targets that would alter the responses of the systems for therapeutic purposes. Therefore, dynamic pathway models are very useful. Several mathematical models of the JAK/STAT pathway are available that are mainly literature-based (11, 12) and focused on nonpathologic systems (13), especially healthy hepatocytes (14, 15). We previously described how a data-based model of JAK2/STAT5 signaling in hematopoietic cells could predict the system's response to perturbations (16). Despite a few exceptions (17), there is a general lack of data-based JAK/STAT mathematical models for pathologic conditions. Moreover, with the exception of rituximab, the currently available therapies for PMBL (18) and cHL (19), based on chemotherapy, radiotherapy, and autologous stem cell transplantation, lack specific molecular targets, thus encouraging studies in this direction.

We report the quantitative analysis of the JAK/STAT pathway in 2 cell lines, MedB-1 (20) and L1236, derived from PMBL and cHL, respectively, by generation of ordinary differentially equation (ODE)–based models and their calibration with time-resolved quantitative experimental data. These studies yielded evidence for major differences and similarities among the 2 tumor entities and facilitated the prediction of potential therapeutic targets.

Materials and Methods

Cell culture

The cHL cell line L1236 was obtained from the German Collection of Microorganisms and Cell Cultures that characterized it by morphology, immunology, DNA fingerprint, and cytogenetics. The PMBL cell line MedB-1 was previously established (20) and characterized by morphology and cytogenetics. Both cell lines were grown in RPMI 1640 supplemented with 10% fetal calf serum, 1% L-glutamine, and 1% penicillin-streptomycin. Before each experiment, cells were starved for 5 hours in RPMI 1640 with 1 mg/mL bovine serum albumin (Sigma-Aldrich Chemie Gmbh). Recombinant human IL13 (R&D Systems) was used as a stimulus in all experiments.

Isolation of human B cells

Primary human B cells were isolated from buffy coats of healthy donors purchased from IKTZ Heidelberg Blood Bank as described in the Supplementary Methods S1.

Real-time PCR

Total RNA was extracted with RNeasy Plus Kit (Qiagen) and 2 μg were reverse transcribed with QuantiTect Rev. Transcription Kit (Qiagen). Quantitative real-time PCR (qRT-PCR) was conducted with the LightCycler 480 System (Roche) and by using probes from the Universal Probe Library (Roche) according to the manufacturer's instructions. The housekeeping gene hypoxanthine phosphoribosyltransferase 1 (HPRT) was used for normalization of all analyzed genes. Tables with primers, probes, and details about the qRT-PCR reaction conditions are supplied in the Supplementary Table S2.

Immunoprecipitations and immunoblotting

Immunoprecipitations (IP), quantitative immunoblotting, and data analysis were done as previously described (21–23), with minor changes (See Supplementary Methods S3).

Flow cytometry

At each time point, cells were centrifuged, washed, and fixed in 2% formaldehyde at room temperature for 30 minutes. After washes, cells were stained with the appropriate antibody for 20 minutes at 4°C, washed again, and acquired at a FACSCalibur Flow Cytometer (BD Biosciences). Data were analyzed with CellQuest Pro software (BD Biosciences). Quantibrite PE (phycoerythrin) Beads (BD Biosciences) were used following manufacturer's instructions to determine the number of receptors on the cell surface. PE molecules per cell were calculated from a standard curve of PE-labeled beads and, assuming a 1:1 monoclonal antibody to receptor ratio, molecules of receptor per cell were then calculated according to the fluorophore to antibody conjugation ratio (1:1 for IL4Ra, 1.8:1 for IL13Ra2).

Antibodies

See Supplementary Methods S4.

ELISA

At the desired time points after IL13 stimulation, cells were centrifuged and supernatant and cell pellets were separated. Cells were lysed and ELISAs were carried out with Human IL-13 Quantikine ELISA Kit (R&D Systems) according to the manufacturer's instructions to detect cell-associated (cell lysate) and extracellular (supernatant) IL13.

Inhibitor

JAK inhibitor I, a JAK2-kinase inhibitor, was purchased from Merck, diluted in dimethyl sulfoxide (DMSO), and used for model validation experiments at a concentration of 160 nmol/L.

Mass spectrometric analysis

Mass spectrometric (MS) analysis was done to measure site-specific phosphorylation degrees of STAT5 and STAT6 in nonstarved cells or cells starved and stimulated with IL13. Following IP of endogenous STATs, proteins were separated on SDS-PAGE and in gel digested with trypsin (STAT5) or AspN/LysC (STAT6) as described (24). MS analysis was done using a nanoAcquity UPLC (Waters) coupled to an LTQ-Orbitrap XL (Thermo) as described (25) for STAT5 or to a QTOF-2 (Waters/Micromass) for STAT6. Site-specific phosphorylation degree was determined in a label-free manner for STAT6 and by isotope dilution analysis with isotopically labeled peptide/phosphopeptide standards for STAT5. Data were analyzed using MassLynx V4.1, Xcalibur 2.0.6, and MASCOT 2.2.2.

Gene expression arrays

After starvation, MedB-1 and L1236 cells were stimulated with 20 and 40 ng/mL IL13, respectively; unstimulated cells were used as control. Samples were collected over a period of 12 hours after stimulation and RNA was analyzed on Human Gene 1.0 ST Arrays (Affymetrix). Data were analyzed, first, by using a standard approach and, second, by using the GraDe algorithms (ref. 26; details in Supplementary Methods S5). Data are available from the National Center for Biotechnology Information Gene Expression Omnibus, accession ID GSE23591.

Mathematical modeling

The ODE-based models were developed and calibrated using the MATLAB toolbox PottersWheel 2.0.47 (ref. 27; Supplementary Methods S6). To find optimal parameter values and to study parameter variability in terms of structural identifiability, 1,000 parameter estimations for randomly selected initial points were carried out for each of the 2 models (MedB-1 model and L1236 model).

Identifiability analysis

Structural identifiability analysis of each mathematical model was done on the best 10% of the 1,000 parameter estimations through analysis of the distribution of parameter estimates and by Mean Optimal Transformations Approach (MOTA; ref. 28). To visualize the variability of the estimated model dynamics corresponding to the distribution of parameter estimates, the 10% best trajectories were displayed for each of the model variables.

Sensitivity analysis

Sensitivity analysis was done as previously described (21) by varying each parameter of the model individually by about 1% of about its estimated value and calculating the relative changes in gene expression, represented in the model by relative changes in the area under the curve from time 0 to 100 minutes of the CD274mRNA trajectory.

Proliferation assay

Cells in cultivation medium were treated with 80 ng/mL IL13 in the presence or absence of JAK inhibitor I, and proliferation was evaluated at 72 hours with a Multisizer Coulter Counter (Beckman Coulter).

Statistical analysis

Two-tailed t test was used to evaluate the significance of the differences between numbers of molecules per cell in different cell types and to test the efficiency of JAK inhibitor I. Bonferroni correction was applied when carrying out multiple tests. The values of $P < 0.05$ were considered statistically significant; χ^2 tests allowed evaluation of the goodness-of-fit of mathematical models. When $P > 0.01$, the models were not rejected and, if necessary, further selected by likelihood ratio tests as reviewed in ref. 29.

Results

Differences in the stoichiometry of signaling components in lymphoma cells

The abundance of cell surface receptors and downstream pathway components has a strong impact on signal transduction (32, 33) and is frequently altered in tumor cells. IL13-induced signal transduction is mediated by the heterodimeric receptor IL4Ra/IL13Ra1. IL13, however, also binds with high-affinity IL13Ra2 (34), a decoy receptor that does not directly contribute to JAK/STAT signaling. By flow cytometry, we showed that both lymphoma cell lines, MedB-1 (20) and L1236, expressed comparable numbers of IL4Ra molecules per cell on the cell surface whereas IL13Ra2 expression is 4-fold higher in L1236 than in MedB-1 cells (Fig. 1 and Supplementary Fig. S11). A direct comparison with receptor expression on CD19^{+} B cells from healthy donors (control cells) was not possible, as the signal was below the detection limit.

The stoichiometry of major components of the JAK/STAT signaling cascade in the 2 lymphoma cell lines and in control cells was determined by quantitative immunoblotting (Supplementary Figs. S12–S14). As shown in Fig. 1, the levels of the signaling components are significantly altered in the 2 lymphoma cell lines compared with controls. Both lymphoma cell
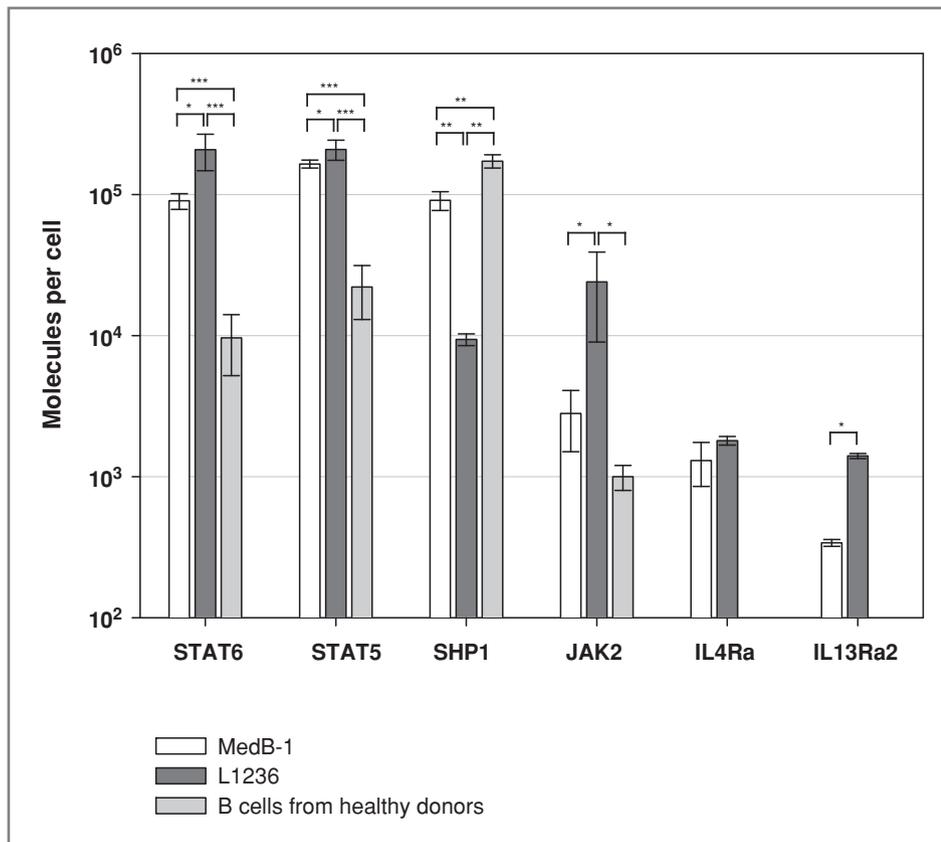
Figure 1. Altered stoichiometry in 2 lymphoma entities compared with B cells from healthy donors (controls). Numbers of molecules per cell for STATs, SHP1, and JAK2 were determined by quantitative immunoblotting (Supplementary Figs. S11–S13), using dilution series of GST-tagged recombinant proteins as reference (Supplementary Methods S3), and capturing the chemiluminescent signal in nonsaturating conditions by CCD camera and quantifying it by LumiAnalyst software. Surface receptor levels were measured by flow cytometry (Supplementary Fig. S10) using Quantibrite PE Beads as references. In controls, the amounts of IL4Ra and IL13Ra2 on the cell surface were below the detection level. Error bars represent SDs of 3 or more replicates. Bonferroni-corrected 2-tailed t test was conducted for statistical significance (*, $P < 0.05$; **, $P < 0.001$; ***, $P < 0.0001$).

lines show a major increase in STAT molecules. Control cells contain approximately 10,000 STAT6 and 22,000 STAT5 molecules per cell. In comparison, MedB-1 cells harbor approximately 9-fold more STAT6, approximately 7-fold more STAT5 and L1236 cells, approximately 22-fold more STAT6, and approximately 9-fold more STAT5. MedB-1 cells, with approximately 3-fold more JAK2 and approximately 2-fold less SHP1, display only minor alterations compared with the 1,000 JAK2 molecules per cell and 173,000 SHP1 molecules per cell of controls. In contrast, L1236 cells show much higher divergence, harboring approximately 25-fold more JAK2 and approximately 18-fold less SHP1. These results indicate that the stoichiometry of receptors and signaling components not only shows quantitative aberrances in lymphoma cells compared with controls but also enables discrimination between different lymphoma types.

### Identification of the STAT family member induced by IL13

The respective roles of STAT5 and STAT6 in the pathway induced by IL13 have been discussed controversially (1, 2, 4, 7, 10). To establish which STAT molecule is primarily transducing the signal initiated by IL13 in our cell systems, the phosphorylation levels of STAT5 and STAT6 in response to IL13 stimulation were examined. Surprisingly, only STAT5 phosphorylation showed a dose-dependent transient increase following IL13 treatment whereas STAT6 phosphorylation did not increase substantially (Fig. 2A and B). The analysis by MS revealed that in normal culture conditions, the levels of activated STAT6 (pSTAT6) are 80% to 90% in both cell types

(Supplementary Fig. S15A and B), explaining the still high levels of STAT6 phosphorylation observed by immunoblotting after starvation. In contrast, the phosphorylation degree of STAT5 achieved by starvation is close to zero (Fig. 2C and Supplementary Fig. S15C). Stimulations of MedB-1 cells with 20 ng/mL IL13 for 40 minutes triggered phosphorylation of STAT5 that is 63% of the total (Fig. 2C), whereas in L1236 cells stimulated with 40 ng/mL IL13 pSTAT5 levels after 40 minutes were 30% of the total STAT5 amounts (Supplementary Fig. S15C). Because of the absence of a major effect of IL13 stimulation on STAT6 phosphorylation, only STAT5 was considered for further analysis.

Time-resolved analyses of IL13 target genes in lymphoma cell lines

To identify at a genome-wide level, the effect of IL13 on gene expression and on biological processes over 12 hours (long-term response) and over 2 hours (early response), we conducted time-resolved expression profiling in MedB-1 and L1236 cells. One hundred seventy-four long-term response genes were detected in MedB-1 cells and 113 in L1236 cells (Supplementary Fig. S16 and Table S16), of which 16 are in common (Supplementary Table S17). The time-courses of 2 of these genes are shown exemplarily (Fig. 3A). Interestingly, molecular functional analysis showed that the IL13-induced genes include many positive (JAK2, STAT3, STAT4, STAT5A, STAT5B) and negative (CISH, SOCS1, SOCS2, SOCS3) regulators of the JAK/STAT pathway in MedB-1 cells, but they include only 2 genes (IL6 and CISH) in L1236 cells. By using the GraDe approach (26), we show that in MedB-1 cells genes involved in

Figure 2. IL13 induces activation of STAT5, but not of STAT6, in MedB-1 cells. Quantitative immunoblotting detection followed by quantification of chemiluminescent signal by LumiAnalyst software, of pSTAT5 (A) and pSTAT6 (B) over time upon IL13 stimulation. Data from 3 different experiments were normalized and averaged. Error bars are derived from linear error models (Supplementary Methods S3). C, measurement of STAT5 phosphorylation degree before and after (40 minutes) IL13 treatment (20 ng/mL) by MS analysis done with labeled internal peptide/phosphopeptide standards. Chromatograms of endogenous peptides are shown. The results are expressed in percentage of total STAT5.
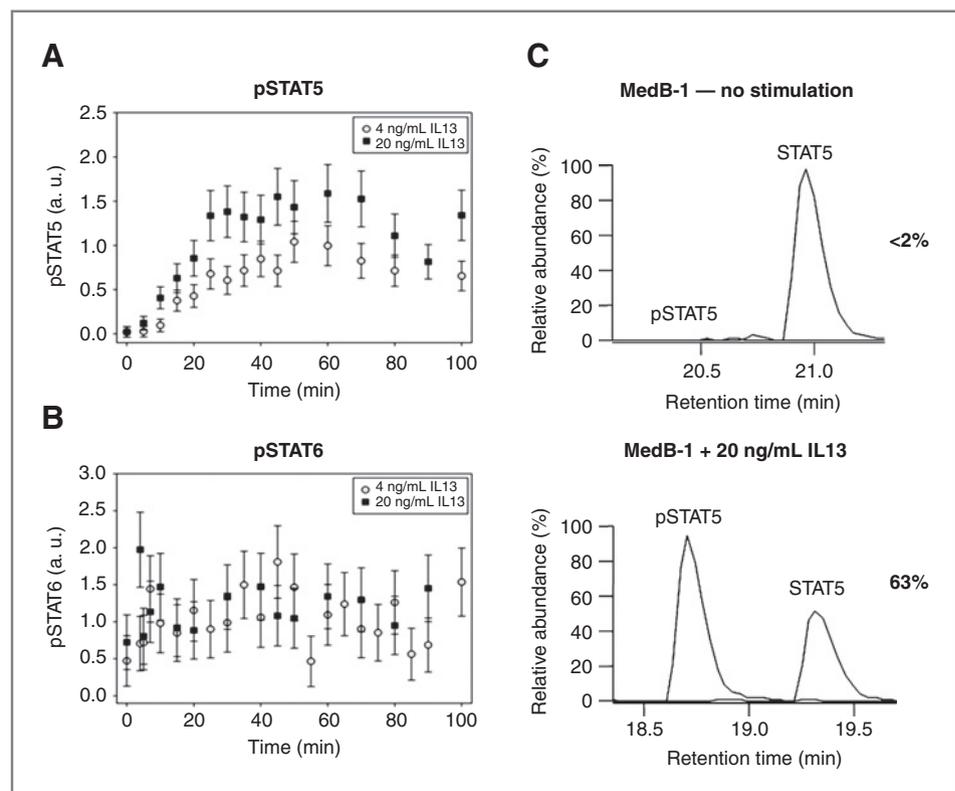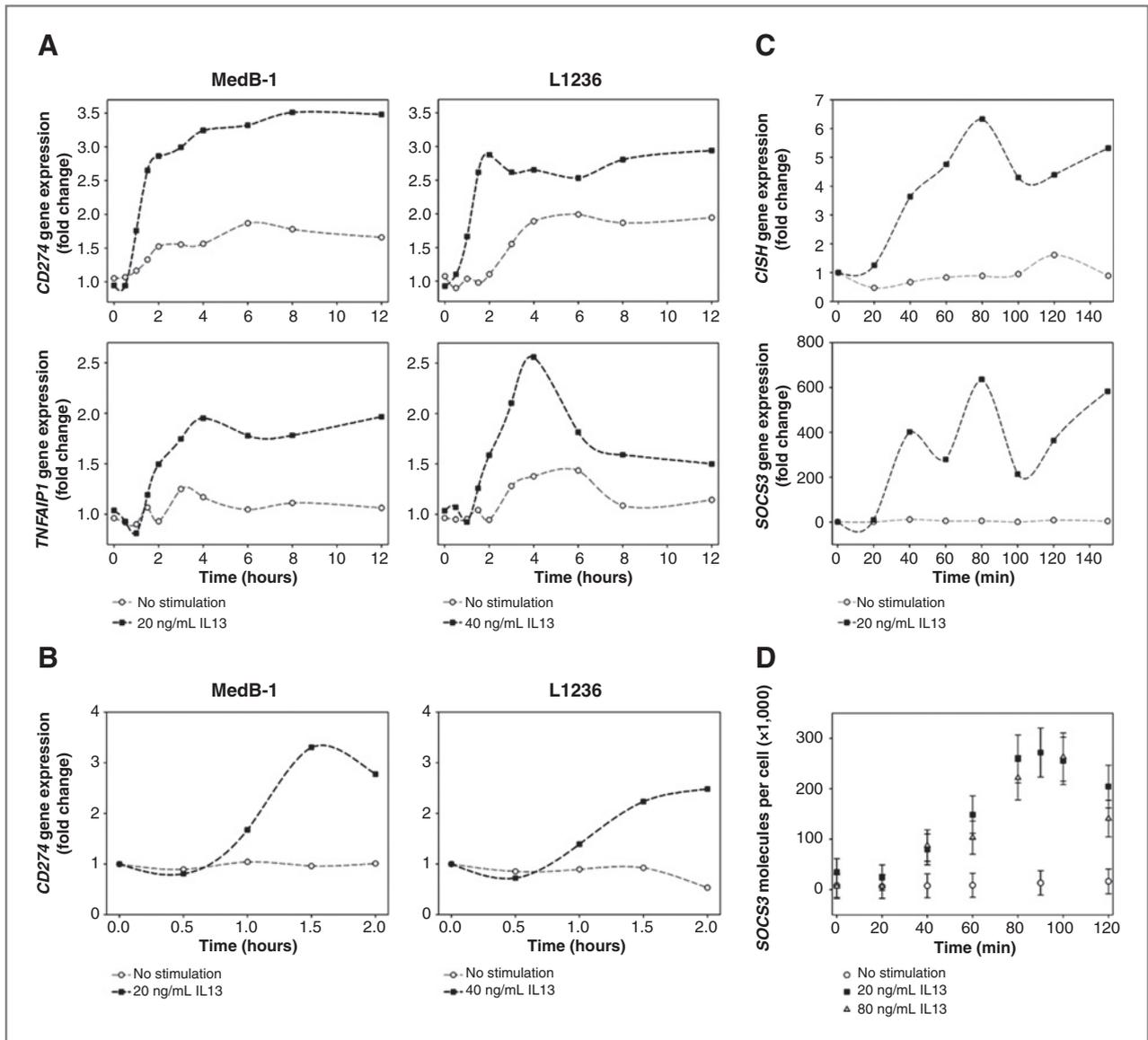
Figure 3. Gene expression analysis and SOCS3 protein induction. A, gene expression array results for 2 commonly upregulated IL13-sustained genes (*CD274* and *TNFAIP1*) in MedB-1 and L1236 cells. Time-courses of nonstimulated (gray) and stimulated (black) cells are represented. B, array validation by qRT-PCR of *CD274* gene expression (2 hours). The displayed qRT-PCR data are the average of 2 technical replicates. C, time-courses of *CISH* and *SOCS3* gene expression in MedB-1 cells analyzed by qRT-PCR using LightCycler 480. The displayed data are the average of 2 technical replicates. Experiments were repeated 3 times with comparable results. The dashed lines represent spline interpolation. D, summary of 3 time-course experiments in which SOCS3 protein induction in MedB-1 cells was detected by quantitative immunoblotting. Band chemiluminescent signal quantification was conducted with LumiAnalyst software. Error bars are derived from a liner error model (Supplementary Methods S3).

metabolic and biosynthetic processes, cell communication, signal transduction, and cell differentiation are significantly upregulated whereas in L1236 cells primarily genes involved in positive regulation of cell death, signal transduction, and developmental processes are upregulated (Supplementary Fig. S18). The analysis of the early response revealed that 190 genes in MedB-1 cells and 141 genes in L1236 cells are upregulated (Supplementary Fig. S16 and Table S16), and of these, 11 genes are common (Supplementary Table S17). Among the common genes, *CD274* is of prime interest because of its clinical relevance (35) and was validated by qRT-PCR as

shown in Fig. 3B, thus providing a readout of JAK/STAT pathway activation in both lymphoma cell lines.

To confirm the results of the expression profiling for major negative regulators of the JAK/STAT pathways, we monitored by qRT-PCR the expression of *CISH* and *SOCS3* (36, 37) over 2 hours upon IL13 stimulation. In line with expression profiling results, these genes showed strong induction in MedB-1 cells (Fig. 3C) but not in L1236 cells. Furthermore, the induction of the SOCS3 protein was investigated by quantitative immunoblotting and could be detected in MedB-1 (Fig. 3D and Supplementary Fig. S19) but not in L1236 cells. Thus, we
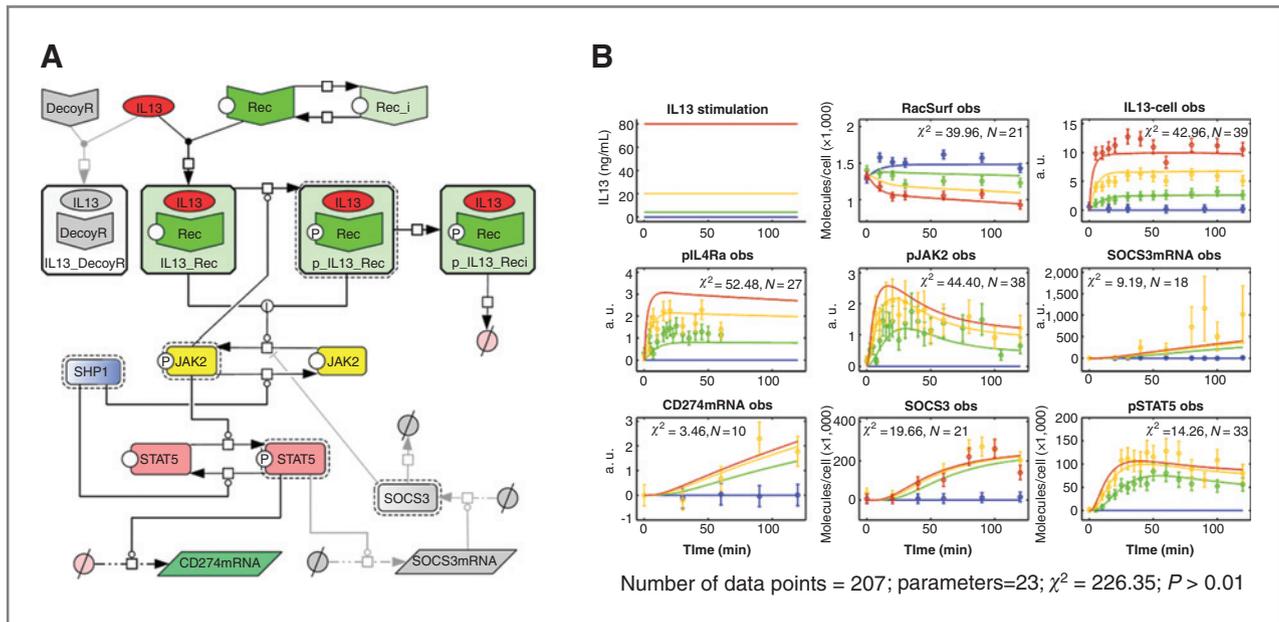
Figure 4. Mathematical models can represent experimental data. A, process diagram of MedB-1 dynamic signaling network model consisting of reactions (arrows) with enzymatic, mass action, or custom kinetics. Round-headed arrows indicate reaction catalysis, whereas bar-ended arrows reaction inhibition. IL13 is used as input function of the system. Reactions and species colored in gray are omitted in the L1236 model. B, data (circles) and trajectories of the best MedB-1 parameter estimation obtained by using the MATLAB toolbox PottersWheel. obs, observations.

established that SOCS3 constitutes a negative feedback loop for JAK/STAT signaling in MedB-1 cells but surprisingly not in L1236 cells.

Developing dynamic models of the JAK/STAT pathway in lymphoma cells

On the basis of the established knowledge, we developed and calibrated 2 structurally similar models for the JAK/STAT pathway in MedB-1 and L1236 cells, the MedB-1 model and the L1236 model, respectively, that are represented as process diagrams (38) in Fig. 4A. These models are based on ODEs and include mass action and enzymatic and custom kinetics of the reactions (see Supplementary Text S7 for model description). To capture reactions at the receptor level, we experimentally determined ligand and receptor dynamics. To ensure the validity of setting the model input as constant, we experimentally confirmed by ELISA that the concentration of IL13 in the medium of treated or untreated MedB-1 and L1236 cells remained constant over time (Supplementary Fig. S20A and B). Furthermore, we measured by ELISA cell-associated IL13 levels over time (Supplementary Fig. S20C and D). In addition, we detected by flow cytometry a dose-dependent reduction of receptors on the cell surface (Supplementary Fig. S21) in both cell lines. To select and calibrate the mathematical models, we analyzed by time-resolved quantitative immunoblotting IL13-induced phosphorylation of IL4Ra, JAK2 (Supplementary Fig. S22) and STAT5 (Fig. 2A and Supplementary Fig. S23). We observed that phosphorylation was rapidly induced and sustained over 2 hours in both cell lines, not decreasing to basal levels during the observation period. This effect was more pronounced in

L1236 than in MedB-1 cells (see Supplementary File II for MedB-1 and III for L1236 model calibration data). To describe the measured dynamic behaviors, the addition of the IL13Ra2 receptor (DecoyR) was required for the MedB-1 model, as shown by a likelihood ratio test (Supplementary Fig. S24) but not necessary for the L1236 model. Another difference in the 2 models resides in the already mentioned lack of SOCS3-mediated negative feedback in L1236 cells (Fig. 4A). The calibrated trajectories of the best models, selected according to the goodness-of-fit using χ^2 tests and $P > 0.01$, are shown in Fig. 4B for MedB-1 and in Supplementary Fig. S25 for L1236 cells. Besides one exception, that the peak of activation of STAT5 at 40 to 60 minutes cannot be fully represented by L1236 model, both models represent well the respective experimental data. We tested several alternative model structures. Examples of the models rejected on the basis of the results of the χ^2 tests are presented in the Supplementary Fig. and Text S26.

To reliably predict the system behavior, it is important to have a structurally identifiable set of parameter values. Therefore, we investigated the distributions of the parameter estimates. The analysis in Fig. 5A revealed that the MedB-1 model is structurally identifiable for 18 of 23 parameters. The quantitative determination of the STAT5 phosphorylation degree by MS and the subsequent conversion of relative units of the STAT5 phosphorylation time-courses to absolute numbers of molecules per cell rendered the STAT5_phosphorylation parameter, previously among the nonidentifiable ones, structurally identifiable. The remaining nonidentifiable parameters are related to mRNA expression of *SOCS3* and *CD274*, as the absolute amounts of mRNA
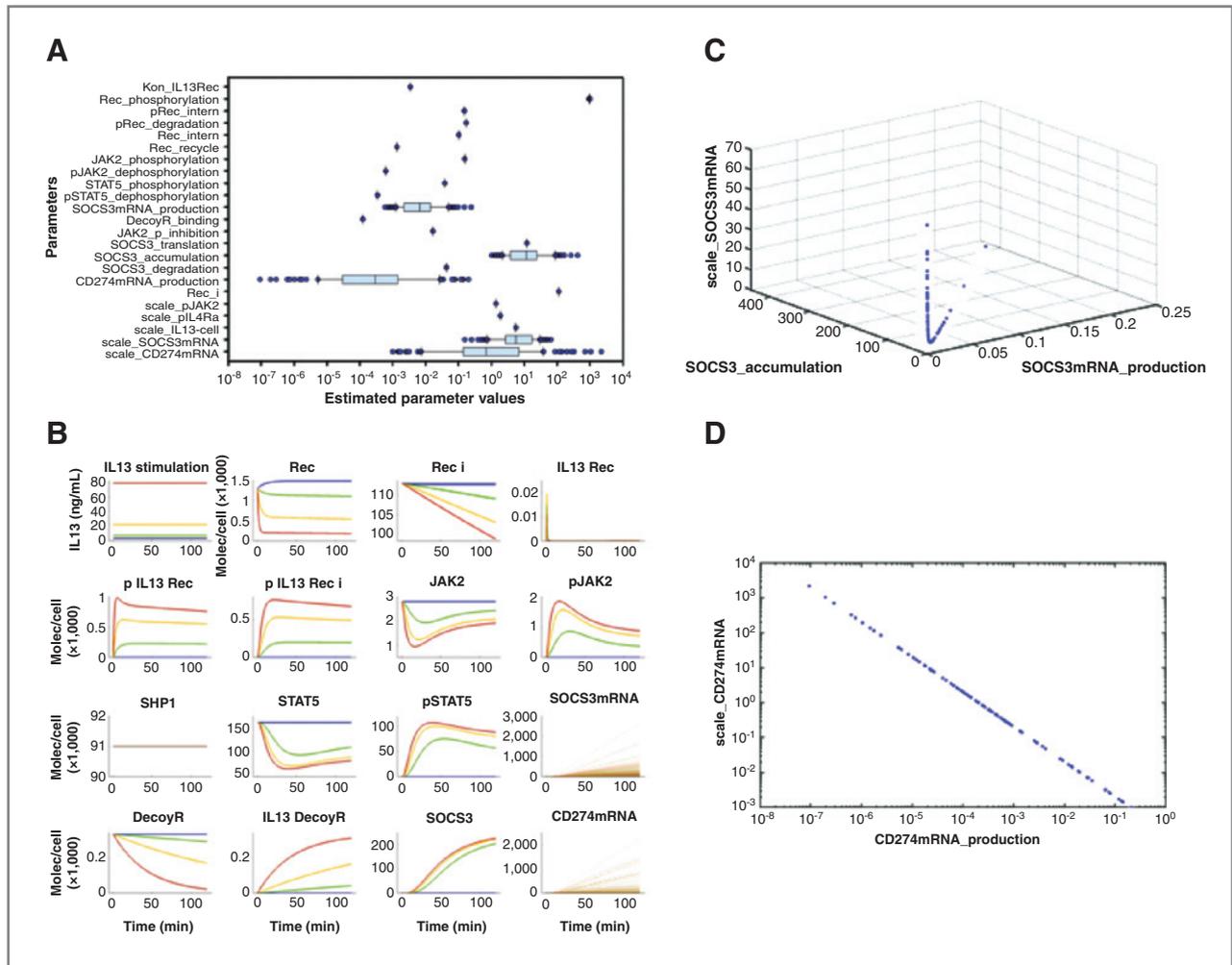
Figure 5. Structural identifiability analysis of the MedB-1 model. Parameter distribution, highlighting the nonidentifiable parameters (larger boxes) (A), and trajectories (B) of 10% best of 1,000 parameter estimations. Relation of the 3 SOCS3-associated (C) and of the 2 CD274-associated (D) parameters. The MATLAB toolbox PottersWheel was used for this analysis.

molecules expressed were not addressable. In line with these parameter nonidentifiabilities, the trajectories for SOCS3mRNA and CD274mRNA show strong variation for different parameter values. For all other variables, the model trajectories are almost identical with each other for the 100 best parameter estimates (Fig. 5B). Interestingly, the MOTA analysis (28) of the MedB-1 model revealed a nonlinear relationship of the 3 nonidentifiable SOCS3-related parameters (Fig. 5C) and of the 2 CD274-associated parameters (Fig. 5D). These analyses carried out with the L1236 model gave comparable results. Of 16 parameters, the 2 nonidentifiable ones, which are related to CD274, correlate with each other (Supplementary Fig. S27). The high number of identifiable parameters in both models, resulting from a large number of experimental data points compared with model parameters, substantiates the fact that overparameterization was not a major issue and therefore our models can be used to infer properties of the system and to predict the system behavior upon small changes in parameter values.

Model prediction and experimental validation of targets for intervention

To identify which components of the pathway are primarily responsible for changes in gene expression, we conducted sensitivity analyses of parameter changes on CD274mRNA (Fig. 6A and B). Surprisingly, DecoyR, DecoyR_binding, pRec_degradation, and Rec_phosphorylation had no effect on the integrated response of CD274mRNA. Of the 2 negative regulators in MedB-1 cells, the constitutively expressed SHP1, has a higher negative impact. As possible therapeutic targets, we focused on major parameters positively influencing *CD274* mRNA expression. Interestingly, we observed that in L1236 cells several parameters (STAT5, JAK2, Rec_i, STAT5_phosphorylation, JAK2_phosphorylation, Rec_recycle) were eligible to be targeted to obtain a significant reduction in *CD274* mRNA whereas in MedB-1 cells only 3 parameters (STAT5, JAK2, and STAT5_phosphorylation) were predicted as targets. These results indicate that IL13-induced gene expression in L1236 cells is more susceptible to changes than in MedB-1 cells.
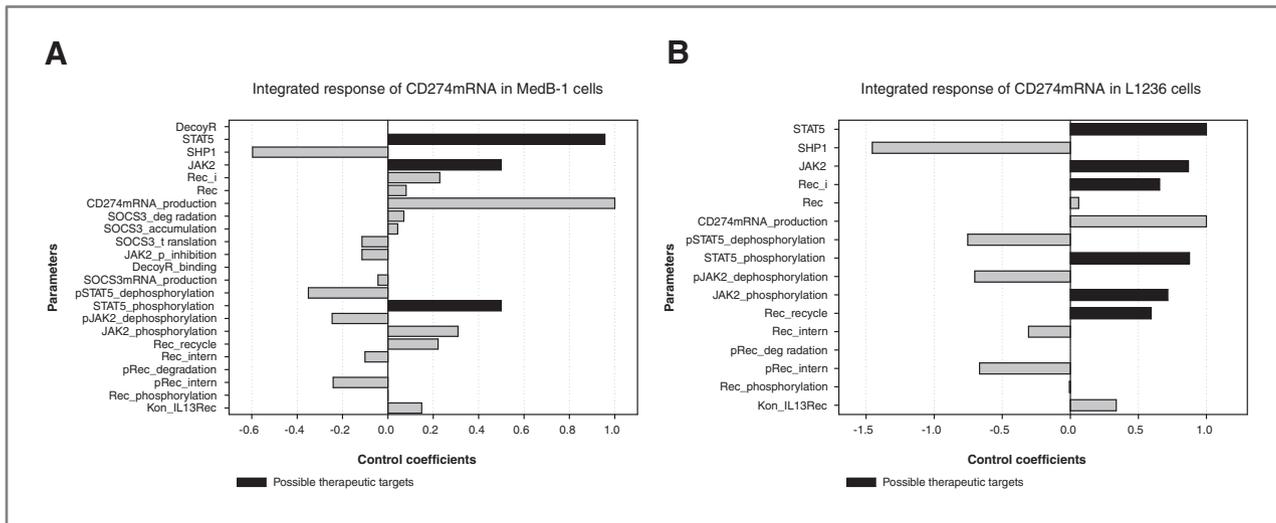
Figure 6. Sensitivity analysis of integrated response of CD274mRNA in MedB-1 (A) and L1236 (B) cells conducted with the MATLAB toolbox PottersWheel. The control coefficients indicate the relative change in CD274mRNA integrated response upon relative changes in the initial values of the other parameters. The analysis is done on small parameter changes (±1% of their value). Possible targetable parameters are represented by black bars.

Our sensitivity analysis indicated the parameter STAT5_phosphorylation as a possible drug target in both cell systems. To experimentally validate the predictions of our mathematical models, we tested the effect on pSTAT5 of the inhibition of this reaction, which is directly dependent on the kinase activity of JAK2. Among the several JAK2 kinase inhibitors available, we selected JAK inhibitor I because it achieves a reduction in STAT5 phosphorylation at relatively low doses (160 nmol/L vs. 200 μmol/L of other inhibitors) and without evident signs of cell toxicity. For optimal experimental design, we used the models, with fixed parameters, to quantitatively predict the effect of JAK inhibitor I on the kinetics of STAT5 phosphorylation in cases of 50%, 80%, or 95% reduction in the STAT5_phosphorylation parameter in MedB-1 (Fig. 7A) and L1236 (Supplementary Fig. S28) cells. The model predicted that the inhibitor reduces the peak amplitude and the time to peak of pSTAT5.

For experimental confirmation, MedB-1 cells were incubated for 1 hour with the JAK inhibitor I in DMSO or DMSO alone (control) and were subsequently stimulated with 20 ng/mL IL13. Samples were collected over 2 hours after stimulation and analyzed for phosphorylation of STAT5 (Fig. 7B and C). The obtained data mirrored the model predictions, as the fixed MedB-1 model could simultaneously represent the data sets derived from inhibitor- and control-treated cells. The model suggested that the inhibitor reduced the STAT5_phosphorylation reaction by 96%. In line with model predictions, STAT5 phosphorylation time of peak shifted from 40 to 80 minutes and its peak amplitude was reduced by approximately 90%. In addition, the effect of JAK inhibitor I on gene expression was evaluated, showing that 100 minutes post–IL13 stimulation of MedB-1 cells the expression of *SOCS3* was reduced by approximately 96% and *CD274* by approximately 57% (Fig. 7D). This is in agreement with the sensitivity analysis indicating that inhibition of STAT5_phosphoryla-

tion causes a reduction of 50% in the integrated response of CD274mRNA (Fig. 6A). Moreover, we showed that JAK inhibitor I affects the proliferation of MedB-1 and L1236 cells (Fig. 7E). Our results showed that, as predicted by our models, the inhibition of STAT5_phosphorylation reaction reduces STAT5 activation and *CD274* expression and negatively affects cell proliferation.

Discussion

We identified through establishment of data-based mathematical models major similarities and differences in the dynamic behavior of the JAK/STAT pathway in 2 lymphoma entities.

Previous cytogenetic based (39, 40) and semiquantitative approaches using immunohistochemistry, qRT-PCR, immunoblotting, and ELISA (1, 41, 42) provided evidence for altered STAT, JAK2, and SHP1 levels in lymphomas compared with normal cells. We extended those studies and showed by determining the number of molecules per cell of proteins involved in the JAK/STAT pathway that the stoichiometry of signaling components significantly differs not only between lymphomas and B cells from healthy donors but also between MedB-1 and L1236 cells. L1236 cells harbor at the same time more JAK2 and less SHP1 than MedB-1 cells and do not induce negative regulators such as *CISH* and *SOCS3* during the early response, suggesting a more aggressive behavior of L1236 cells. On the contrary, L1236 cells have a longer duplication time than MedB-1 cells. By mathematical modeling, we showed that despite apparent lack of efficient negative regulation, the JAK/STAT pathway in L1236 is highly susceptible to perturbations. Therefore, we hypothesize that the good clinical outcome for cHL patients is partly due to off-target therapy effects that affect one of our predicted targets in the JAK/STAT pathway.
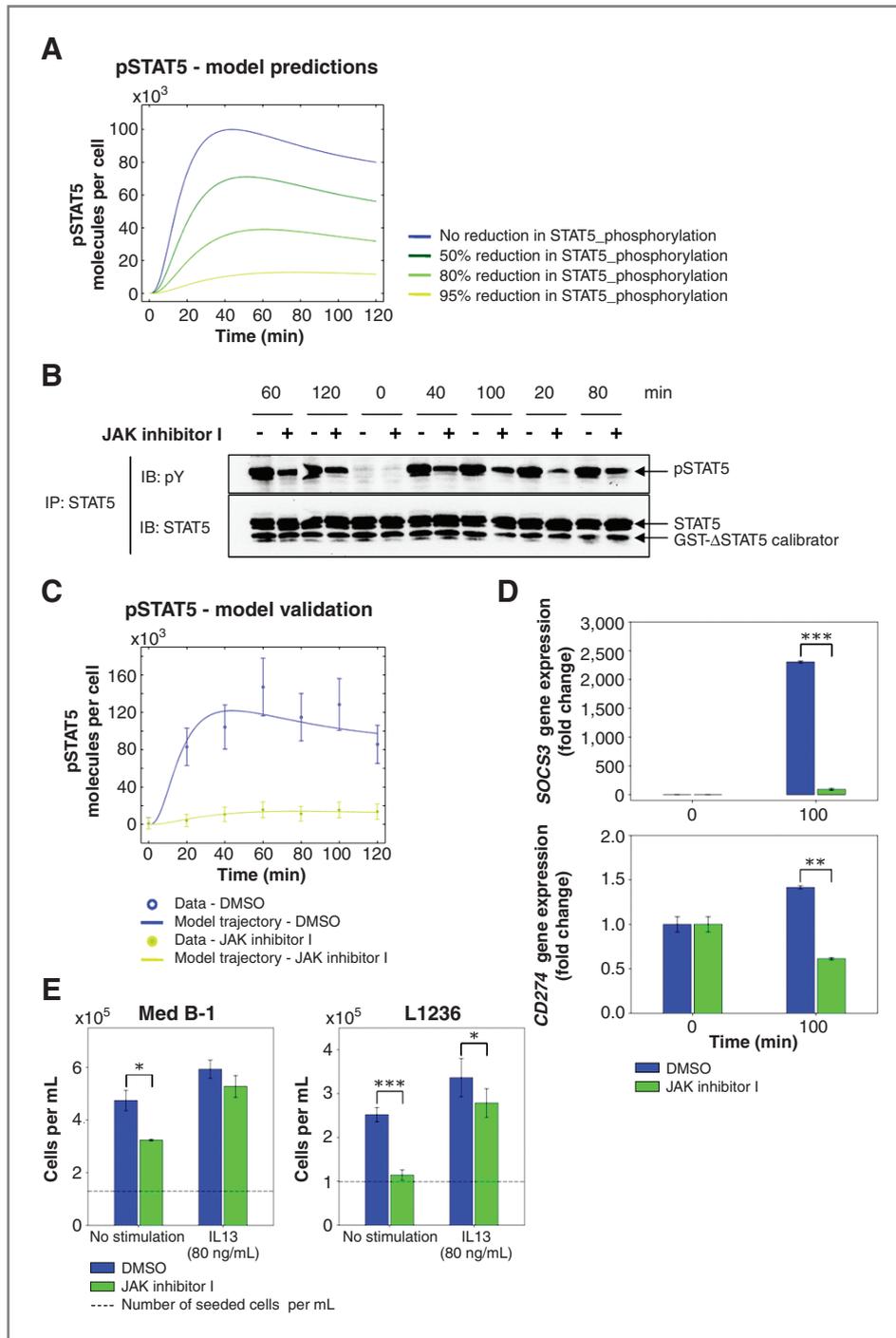
Figure 7. MedB-1 model predictions and validation. A, model predictions of pSTAT5 kinetics in case of 50%, 80%, and 95% reduction of the STAT5_phosphorylation parameter. B and C, model validation. B, immunoblotting evidence of pSTAT5 reduction upon 160 nmol/L JAK inhibitor I treatment (1 hour preincubation followed by 20 ng/mL IL13 stimulation). Band chemiluminescent signal quantification was conducted with LumiAnalyst software. C, graphic representation of (B), including experimental data and simultaneous model representation of the 2 conditions, DMSO and JAK inhibitor I in DMSO. Error bars are derived from a linear error model (Supplementary Methods S3). The experiment was repeated 3 times with comparable results. D, effect of JAK inhibitor I on IL13-induced SOCS3 and CD274 gene expression, determined by qRT-PCR using LightCycler 480, and (E) on proliferation (see Materials and Methods for details). The error bars derive from triplicates. Two-tailed t test was carried out for statistical significance (*, $P < 0.05$; **, $P < 0.005$; ***, $P < 0.0005$).

Furthermore, array analysis of long-term gene expression showed that the IL13-mediated induction of positive and negative regulators of the JAK/STAT pathway is abundant in MedB-1 cells but is limited to only 2 genes in L1236 cells. Moreover, analysis of biological processes induced by IL13 showed a very strong and survival-oriented response in MedB-1 cells, including genes involved in cell activation, differentiation, and communication and signal transduction, but rather conflicting responses in L1236 cells, such as

positive regulation of developmental processes, signal transduction, and cell death. A possible explanation is that in L1236 cells, IL13 alone is not sufficient to determine cell-fate decisions and that L1236 cells have retained a more tightly controlled system than MedB-1 cells.

For the identification of reactions that have a differential impact in tumor cells compared with normal cells, a dynamic pathway model for the IL13/JAK2/STATs pathway in normal B cells would be required. However, because of the limited

biological material obtained when isolating B cells from healthy donors (as described in Materials and Methods), it was not possible with the available techniques to generate the necessary quantitative time-resolved data. Nevertheless, our mathematical modeling approach enabled us to identify major differences in reactions and system properties in the 2 lymphoma cell lines. First, although the IL13Ra2 decoy receptor is expressed at higher levels on the cell surface of L1236 cells, there the decoy function has less impact on IL13 signaling than on MedB1-cells. Second, the peak of STAT5 phosphorylation is not fully represented by the L1236 model and we speculate that factors outside the pathway, and not yet considered in the model, modulate these responses. In fact, cross-talks between STAT5 and other pathways, in particular NFκB signaling, have been frequently reported for human lymphomas (43, 44). These cross-talks were confirmed for both cHL- and PMBL-derived cell lines by our gene expression analysis showing late upregulation of genes involved in NFκB and MAP-kinase pathways.

The roles of specific STATs for the JAK/STAT pathway in lymphomas have been controversially discussed. We identified STAT5 as the family member that is directly responsive to IL13 in MedB-1 and L1236 cells. In our experimental settings, STAT6 phosphorylation is not significantly increased in response to IL13 stimulation, because it is already present at high levels. On the other hand, JAK2 phosphorylation was reduced by starvation and induced by IL13 stimulation agreeing with previous reports (1), suggesting that STAT6 activation is only partially JAK2-dependent if not JAK2-independent. According to our expression profiling analysis, other STATs (*STAT3*, *STAT4*, *STAT5A,* and *STAT5B*) are transcriptionally induced upon IL13 stimulation but only in MedB-1 cells. Furthermore, our studies reveal that different negative regulators regulate the IL13-induced JAK/STAT pathway in the 2 cell lines. Despite the lack of functional SOCS1, both cell lines express the phosphatase SHP1 and only MedB-1 shows induction of SOCS3.

Our sensitivity analysis identified major reactions and molecules as candidate therapeutic targets for both analyzed lymphoma types, and we experimentally confirmed one of them, STAT5_phosphorylation, by targeted inhibition.

In summary, through a systems biology approach, we provide evidence for similarities and differences between cHL and PMBL, concerning the IL13/JAK2/STATs pathway. The mathematical models we established represent important tools to quantitatively predict the behavior of pathway components upon alteration of one or more components and provide guidance for the rational design of therapeutic molecules.

Disclosure of Potential Conflicts of Interest

Acknowledgments

Grant Support

References

1. Guiter C, Dusanter-Fourt I, Copie-Bergman C, Boulland ML, Le Gouvello S, Gaulard P, et al. Constitutive STAT6 activation in primary mediastinal large B-cell lymphoma. Blood 2004;104:543–9.
2. Skinnider BF, Elia AJ, Gascoyne RD, Patterson B, Trumper L, Kapp U, et al. Signal transducer and activator of transcription 6 is frequently activated in Hodgkin and Reed-Sternberg cells of Hodgkin lymphoma. Blood 2002;99:618–26.
3. Melzner I, Bucur AJ, Bruderlein S , Dorsch K, Hasel C, Barth TF, et al. Biallelic mutation of SOCS-1 impairs JAK2 degradation and sustains phospho-JAK2 action in the MedB-1 mediastinal lymphoma line. Blood 2005;105:2535–42.
4. Weniger MA, Melzner I, Menz CK, Wegener S, Bucur AJ, Dorsch K, et al. Mutations of the tumor suppressor gene SOCS-1 in classical Hodgkin lymphoma are frequent and associated with nuclear phospho-STAT5 accumulation. Oncogene 2006;25:2679–84.
5. Meier C, Hoeller S, Bourgau C, Hirschmann P, Schwaller J, Went P, et al. Recurrent numerical aberrations of JAK2 and deregulation of the JAK2-STAT cascade in lymphomas. Mod Pathol 2009;22:476–87.
6. Martini M, Hohaus S, Petrucci G, Cenci T, Pierconti F, Massini G, et al. Phosphorylated STAT5 represents a new possible prognostic marker in Hodgkin lymphoma. Am J Clin Pathol 2008;129:472–7.
7. Rolling C, Treton D, Pellegrini S, Galanaud P, Richard Y. IL4 and IL13 receptors share the gamma c chain and activate STAT6,

STAT3 and STAT5 proteins in normal human B cells. FEBS Lett 1996;393:53–6.
8. Murata T, Puri RK. Comparison of IL-13- and IL-4-induced signaling in EBV-immortalized human B cells. Cell Immunol 1997;175:33–40.
9. Kapp U, Yeh WC, Patterson B, Elia AJ, Kagi D, Ho A, et al. Interleukin 13 is secreted by and stimulates the growth of Hodgkin and Reed-Sternberg cells. J Exp Med 1999;189:1939–46.
10. Scheeren FA, Diehl SA, Smit LA, Beaumont T, Naspetti M, Bende RJ, et al. IL-21 is expressed in Hodgkin lymphoma and activates STAT5: evidence that activated STAT5 is required for Hodgkin lymphomagenesis. Blood 2008;111:4706–15.
11. Zi Z, Cho KH, Sung MH, Xia X, Zheng J, Sun Z. *In silico* identification of the key components and steps in IFN-gamma induced JAK-STAT signaling pathway. FEBS Lett 2005;579:1101–8.
12. Guerriero ML, Dudka A, Underhill-Day N, Heath JK, Priami C. Narrative-based computational modelling of the Gp130/JAK/STAT signalling pathway. BMC Syst Biol 2009;3:40.
13. Papin JA, Palsson BO. The JAK-STAT signaling network in the human B-cell: an extreme signaling pathway analysis. Biophys J 2004;87:37–46.
14. Yamada S, Shiono S, Joo A, Yoshimura A. Control mechanism of JAK/STAT signal transduction pathway. FEBS Lett 2003;534:190–6.

15. Singh A, Jayaraman A, Hahn J. Modeling regulatory mechanisms in IL-6 signal transduction in hepatocytes. Biotechnol Bioeng 2006;95: 850–62.

16. Swameye I, Muller TG, Timmer J, Sandra O, Klingmuller U. Identification of nucleocytoplasmic cycling as a remote sensor in cellular signaling by databased modeling. Proc Natl Acad Sci U S A 2003;100:1028–33.

17. Won HH, Park I, Lee E, Kim JW, Lee D. Comparative analysis of the JAK/STAT signaling through erythropoietin receptor and thrombopoietin receptor using a systems approach. BMC Bioinformatics 2009;10Suppl 1:S53.

18. Martelli M, Ferreri AJ, Johnson P. Primary mediastinal large B-cell lymphoma. Crit Rev Oncol Hematol 2008;68:256–63.

19. Hamilton A, Gallipoli P, Nicholson E, Holyoake TL. Targeted therapy in haematological malignancies. J Pathol 2010;220:404–18.

20. Möller P, Bruderlein S, Strater J, Leithauser F, Hasel C, Bataille F, et al. MedB-1, a human tumor cell line derived from a primary mediastinal large B-cell lymphoma. Int J Cancer 2001;92:348–53.

21. Schilling M, Maiwald T, Hengl S, Winter D, Kreutz C, Kolch W, et al. Theoretical and experimental analysis links isoform-specific ERK signalling to cell fate decisions. Mol Syst Biol 2009;5:334.

22. Vera J, Bachmann J, Pfeifer AC, Becker V, Hormiga JA, Darias NV, et al. A systems biology approach to analyse amplification in the JAK2-STAT5 signalling pathway. BMC Syst Biol 2008;2:38.

23. Schilling M, Maiwald T, Bohl S, Kollmann M, Kreutz C, Timmer J, et al. Quantitative data generation for systems biology: the impact of randomisation, calibrators and normalisers. Syst Biol (Stevenage) 2005;152:193–200.

24. Seidler J, Adal M, Kubler D, Bossemeyer D, Lehmann WD. Analysis of autophosphorylation sites in the recombinant catalytic subunit alpha of cAMP-dependent kinase by nano-UPLC-ESI-MS/MS. Anal Bioanal Chem 2009;395:1713–20.

25. Seidler J, Zinn N, Haaf E, Böhm ME, Winter D, Schlosser A, et al. Metal ion-mobilizing additives for comprehensive detection of femtomole amounts of phosphopeptides by reversed phase LC-MS. Amino Acids 2010. Jun 16. [Epub ahead of print].

26. Kowarsch A, Blöchl F, Bohl S, Saile M, Gretz N, Klingmüller U, et al. Knowledge-based matrix factorization temporally resolves the cellular responses to Il-6 stimulation. BMC Bioinformatics 2010;11–585.

27. Maiwald T, Timmer J. Dynamical modeling and multi-experiment fitting with PottersWheel. Bioinformatics 2008;24:2037–43.

28. Hengl S, Kreutz C, Timmer J, Maiwald T. Data-based identifiability analysis of non-linear dynamical models. Bioinformatics 2007;23: 2612–8.

29. Kreutz C, Timmer J. Systems biology: experimental design. FEBS J 2009;276:923–42.

30. Xiao W, Hong H, Kawakami Y, Kato Y, Wu D, Yasudo H, et al. Tumor suppression by phospholipase C-beta3 via SHP-1-mediated dephosphorylation of Stat5. Cancer Cell 2009;16:161–71.

31. Kim YS, Seo DW, Kong SK, Lee JH, Lee ES, Stetler-Stevenson M, et al. TIMP1 induces CD44 expression and the activation and nuclear translocation of SHP1 during the late centrocyte/post-germinal center B cell differentiation. Cancer Lett 2008;269:37–45.

32. Hagner PR, Schneider A, Gartenhaus RB. Targeting the translational machinery as a novel treatment strategy for hematologic malignancies. Blood 2010;115:2127–35.

33. Nasim MT, Ghouri A, Patel B, James V, Rudarakanchana N, Morrell NW, et al. Stoichiometric imbalance in the receptor complex contributes to dysfunctional BMPR-II mediated signalling in pulmonary arterial hypertension. Hum Mol Genet 2008;17:1683–94.

34. Daines MO, Tabata Y, Walker BA, Chen W, Warrier MR, Basu S, et al. Level of expression of IL-13R alpha 2 impacts receptor distribution and IL-13 signaling. J Immunol 2006;176:7495–501.

35. Zou W. Immunosuppressive networks in the tumour environment and their therapeutic relevance. Nat Rev Cancer 2005;5:263–74.

36. Matsumoto A, Masuhara M, Mitsui K, Yokouchi M, Ohtsubo M, Misawa H, et al. CIS, a cytokine inducible SH2 protein, is a target of the JAK-STAT5 pathway and modulates STAT5 activation. Blood 1997;89:3148–54.

37. Davey HW, McLachlan MJ, Wilkins RJ, Hilton DJ, Adams TE. STAT5b mediates the GH-induced expression of SOCS-2 and SOCS-3 mRNA in the liver. Mol Cell Endocrinol 1999;158:111–6.

38. Kitano H, Funahashi A, Matsuoka Y, Oda K. Using process diagrams for the graphical representation of biological networks. Nat Biotechnol 2005;23:961–6.

39. Joos S, Granzow M, Holtgreve-Grez H, Siebert R, Harder L, Martin-Subero JI, et al. Hodgkin's lymphoma cell lines are characterized by frequent aberrations on chromosomes 2p and 9p including REL and JAK2. Int J Cancer 2003;103:489–95.

40. Feys T, Poppe B, De Preter K, Van Roy N, Verhasselt B, De Paepe P, et al. A detailed inventory of DNA copy number alterations in four commonly used Hodgkin's lymphoma cell lines. Haematologica 2007;92:913–20.

41. Delibrias CC, Floettmann JE, Rowe M, Fearon DT. Downregulated expression of SHP-1 in Burkitt lymphomas and germinal center B lymphocytes. J Exp Med 1997;186:1575–83.

42. Renné C, Willenbrock K, Martin-Subero JI, Hinsch N, Döring C, Tiacci E, et al. High expression of several tyrosine kinases and activation of the PI3K/AKT pathway in mediastinal large B cell lymphoma reveals further similarities to Hodgkin lymphoma. Leukemia 2007;21:780–7.

43. Hinz M, Lemke P, Anagnostopoulos I, Hacker C, Krappmann D, Mathas S, et al. Nuclear factor kappaB-dependent gene expression profiling of Hodgkin's disease tumor cells, pathogenetic significance, and link to constitutive signal transducer and activator of transcription 5a activity. J Exp Med 2002; 196:605–17.

44. Nagy ZS, LeBaron MJ, Ross JA, Mitra A, Rui H, Kirken RA. STAT5 regulation of BCL10 parallels constitutive NFkappaB activation in lymphoid tumor cells. Mol Cancer 2009;8:67.